Infrared Physics and Technology 105 (2020) 103206

Contents lists available at ScienceDirect

Infrared Physics & Technology

journal homepage: www.elsevier.com/locate/infrared

Evaluation and classification of five cereal fungi on culture medium using Visible/Near-Infrared (Vis/NIR) hyperspectral imaging

Yao Lu[a], Wei Wang[a,*], Meigui Huang[b], Xinzhi Ni[c], Xuan Chu[d], Chunyang Li[e]

[a] Beijing Key Laboratory of Optimization Design for Modern Agricultural Equipment, College of Engineering, China Agricultural University, Beijing 100083, China
[b] Department of Food Science and Technology, College of Light Industry and Food Engineering, Nanjing Forestry University, Nanjing 210037, China
[c] Crop Genetics and Breeding Research Unit, USDA-ARS, 2747 Davis Road, Tifton, GA 31793, USA
[d] College of Mechanical and Electrical Engineering, Zhongkai University of Agriculture and Engineering, Guangzhou 510225, China
[e] Institute of Food Science and Technology, Jiangsu Academy of Agricultural Sciences, Nanjing 210014, China

ARTICLE INFO

Keywords:
Hyperspectral imaging
Fungi growth
Early detection
Species discrimination
Principal component analysis (PCA)
Maize agar medium

ABSTRACT

In order to detect and identify fungal infection in cereals timely even at its early stage of spore germination and development, a visible/near-infrared hyperspectral imaging (HSI) system with a wavelength range between 400 and 1000 nm was utilized to determine fungal growth. Five common cereal fungi, *Aspergillus parasiticus*, *Aspergillus flavus*, *Aspergillus glaucus*, *Aspergillus niger* and *Penicillium* sp., were selected and cultivated on Maize Agar medium individually for 6 d, HSI images were captured every 24 h for each fungus. Firstly, to classify the growth days of the five fungi, spectral characteristics were analyzed and principal component analysis (PCA) was performed, from which the growth of each fungus can be roughly divided into four growth stages, i.e., the control group-D1, D2, D3, D4-D6. Then support vector machine (SVM) model of each fungus for inoculation days were established with the first four PCs as inputs. Optimal wavelengths were then selected by successive projection algorithm (SPA) to create corresponding multispectral classification models. Overall results were satisfactory, in which accuracies of *A. niger* and *A. glaucus* were both higher than 95.87%. To further differentiate fungal species as early, the HSI images of five fungi for only one day growth were analyzed, and all five species can be distinguished well with an average accuracy of 98.89% and 0.97 for Kappa coefficient using SPA-SVM method. The results proved that VNIR hyperspectral imaging could be used to evaluate growth characteristic of cereal fungi.

1. Introduction

According to FAO statistics, the amount of grain wasted due to microbial contamination and spoilage in the world reached to 25%, and the main culprit is fungi [1]. During the process of grain storage, fungi multiply rapidly in the humid and warm environment which can lead to health risk and the entrance of mycotoxins into the food chain when consumed by human or livestock [2,3]. Only by observing the growth phase and clarifying the species of infected fungi in time can we take corresponding measures to prevent and control fungal contamination, which is of great significance to ensure grain quality and food safety in downstream industries [4,5].

As one of the world's major food crops, maize is highly susceptible to many mycotoxins, such as aflatoxins and vomitoxin, which are mainly produced by those toxic fungi or non-toxic fungi causing ear rot [6]. Saleemi et al. isolated and identified the fungal species carried in 82 types of maize samples, of which *Aspergillus* accounted for 33%, *Penicillium* accounted for 28% [7]. In addition, Mukanga et al. summarized that the two species are also the leading fungi species causing maize ear rot [8]. As a result, it is of vital importance to study the biological characteristics of *Aspergillus* and *Penicillium*.

Traditional procedure for fungal detection methods such as colony counting and/or microscopic enumeration is time-consuming, laborious and may lead to further biological or chemical contamination [9]. Recent advancement in the new technology - hyperspectral imaging (HSI), as a spectral imaging technique, which can provide both spatial and spectral information simultaneously, have significant advantage over traditional NIR spectroscopic technology in the distribution of the chemical composition of samples [10–13]. Due to its attractive features like nondestructive detection and high efficiency, hyperspectral imaging has become an important identification tool for detecting infections of fungi and contaminations of mycotoxins in maize or other cereals [14,15].

Traditionally, contaminated maize kernels were taken as target

* Corresponding author.
E-mail address: playerwxw@cau.edu.cn (W. Wang).

https://doi.org/10.1016/j.infrared.2020.103206
Received 25 October 2019; Received in revised form 16 January 2020; Accepted 17 January 2020
Available online 19 January 2020
1350-4495/

object, i.e., Williams et al. and Chu et al. evaluated the fungal infection and figured out the changes in fungal infected maize kernels over time [16,17]. However, considering the complexity or variability of the microbial growth process itself, together with the diversity of the conditions of the substrate, i.e. maize grain, it is rather difficult to identify the true growth characteristics of fungi from the mixture of fungi and cereals, either contaminated naturally or artificially under laboratory-controlled condition. Therefore, this study starts with the identification of fungal characteristics growing on ideal culture medium and environment condition, so as to serve as the basis for sequential research on maize seeds infected with fungi.

There have been few publications that detect fungi plated on the culture medium using hyperspectral imaging technique. Williams et al. differentiated three Fusarium spp. which was point-injected into the potato dextrose agar growth for 0–55 h using HSI in the range of 1100–2200 nm and growth for 72–96 h in range of 1000–2498 nm, respectively [18,19]. Yao et al. classified five toxin-producing fungal isolates on fifth day in single or mixture mode using three narrow bands [9]. In a similar study, Sun et al. demonstrated fungal growth of *Botrytis cinerea*, *Rhizopus stolonifera* and *Colletotrichum acutatum* and concluded that the three fungi are most distinguishable at 36 h [20]. Furthermore, Jin et al. classified the toxigenic and atoxigenic strains of *A. flavus* using a hyperspectral image under UV light and halogen light source [21]. Dégardin et al. reported that the reflectance of *A. flavus* colony in different growth periods was significantly different [22]. In addition, Kimuli et al. used hyperspectral imaging to examine the competitive growth of five fungus species in one medium found that *A. niger* grows fastest [23], while Chu et al. focused on the growth of *A. flavus* and *A. parasiticus* on rose bengal medium, which was also informative [24]. All of the aforementioned studies had proved the feasibility of detecting fungal infections using hyperspectral imaging, although novel, focus more on point-inject cultural methods and at specific point growth time. Pouring inoculation method is more in line with the actual infection situation, and it will inevitably show different biological and spectral image characteristics from the point inoculation method. In addition to growth characteristics, the feasibility of more early identification of species, as well as systematically studying the full spectrum and multispectral classification models for the above problems, are all necessary.

Thus, the purpose of this study was to utilize HSI technique to evaluate the growth stages and then classify the species of the five fungi even during their early development, which is of great significance to timely control the fungal infection or mycotoxin contaminations. The specific objectives are to: (1) classify the growth stages of the five fungi qualitatively; (2) establish the fungal growth day discriminant model based on full spectra and multi-spectral data selected by corresponding wavelength extraction method; and (3) explore the feasibility of early identification of different fungi and determine the earliest identifiable time node.

2. Material and methods

2.1. Sample preparation

Five fungi, *A. parasiticus*, *A. flavus*, *A. glaucus*, *A. niger* and *Penicillium* sp., as listed in Table 1, were obtained from the China General Microbiological Culture Collection Center, Beijing, China (CGMCC). The five fungi were purely propagated on PDA medium under the condition of 28 °C for 7 d, and then mature spores with high vigor and consistent activity level were obtained. The fresh conidia on PDA were scraped separately and diluted with sterile distilled water in a sterile environment. With a hamocytometer, the concentration of spore suspension was adjusted to 1×10^6 spore mL^{-1}.

By mixing 1 mL of respective fungal spore suspension with 20 mL of Maize Agar Medium (MAM), five pure fungi samples were obtained. In order to make the fungi samples more uniform, every culture dish was rotated gently and after the sample turned solid it was incubated on the MAM at a constant 30 °C. To compare the growth of fungi, 1 mL of 0.9% sterile saline was inoculated on the same media as control group.

Table 1
Strain number of five fungi used in the experiment.

Num.	Fungal Species	Strain Number of CGMCC
1	*A. parasiticus*	3.6155
2	*A. flavus*	3.2890
3	*A. glaucus*	3.3975
4	*A. niger*	3.6473
5	*Penicillium* sp.	3.3703

The hyperspectral images of five fungus species grown on MAM for 1–6 d were collected with an interval of 24 h. And three identical replicates were performed for each day growth of the five fungi. Hence, 21 hyperspectral images (6 days × 3 replicates + 3 control group) were acquired for each variety of fungi, and 105 hyperspectral images for five species in total.

2.2. Hyperspectral system calibration and imaging acquisition

To acquire hyperspectral images, an ImSpector short wave infrared camera (ImSpector V10, Spectral Imaging Ltd, Oulu, Finland) equipped with a translation stage was used. Individual images were obtained within the spectral range of 380–1012 nm at 5.6 nm resolution. In order to ensure the accuracy of image acquisition, the hyperspectral imager has a distance of 40 cm from the sample and an exposure time of 32 ms, set a translation stage moving speed of 1.2 cm/s, and let the light source be at an angle of 45° to the vertical direction of the sample with translation stage.

During imaging, the petri dishes without lids were placed carefully on the translation stage equipped with a black background plate, and was allowed to pass under the camera lens to capture the HSI images. When the samples entered the field of view, image acquisition would proceed by sequential (line by line) scanning. All of the hyperspectral images acquired by the system contained 284 wavelengths with an image of 688 × 500 pixel resolution for each wavelength.

To remove the dark current effect of the camera and to eliminate the effect of uneven illumination, image calibration was performed for the raw images. A white reference image was acquired from a white reference panel (99.9% reflectance) and a dark reference image was obtained by covering the camera with its own opaque cap (0% reflectance). A relative reflectance images was calculated using Formula 1:

$$R_c = \frac{R - D}{W - D} \times 100\% \quad (1)$$

where *Rc* is the resulting calibration images and *R* is raw acquired images, *W* is the white reference image and *D* is the dark current image [25].

2.3. Image pre-treatment and noise cleaning

Various pretreatments were applied to the hyperspectral image data file to reduce background noise and obtain clean fungal growth images; (1) the original image was cropped to 540 × 540 pixels using the resize function in ENVI to remove background noise; (2) high noise images of the two spectral regions (368–400 nm, 1000–1024 nm) were excluded and the images in the spectral range of 400–1000 nm (284 wavelengths) were retained for analysis; (3) only a circular area, which was smaller than the culture dish, was selected as the ROIs to reduce residual noise; and (4) a forward PCA and its reverse rotation were conducted to reduce the dimensionality, multiple co-linearity and background noise, and the first six PCs which can express more than 99% of the original spectral information were chosen to perform

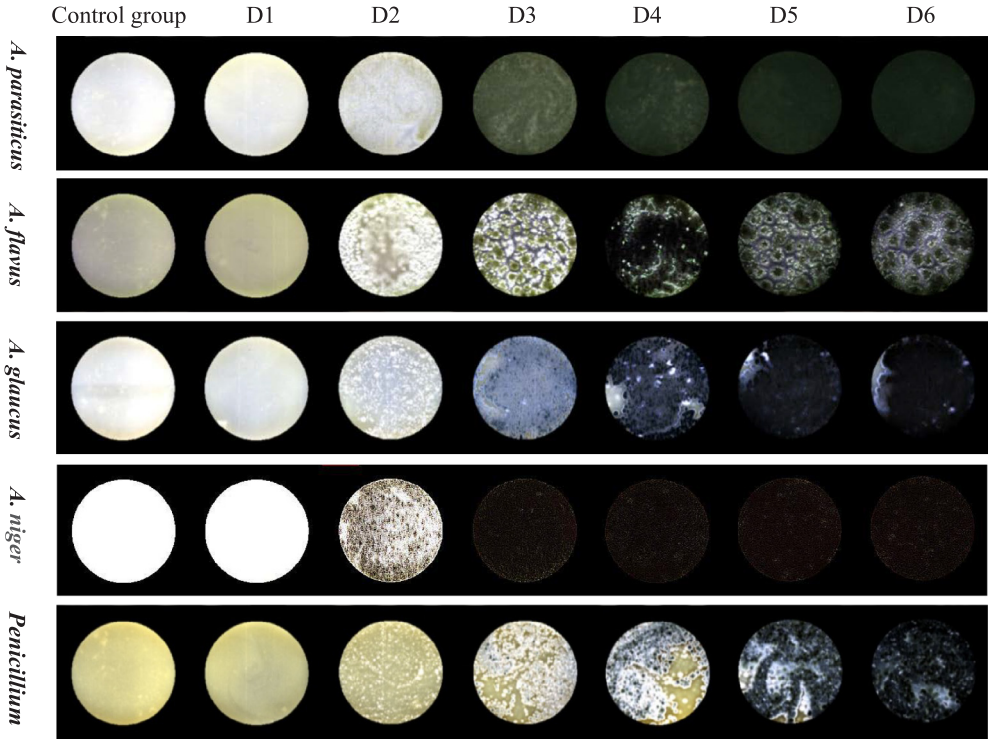

Fig. 1. Pseudo-color images of five fungi growth on maize agar medium for six days.

inverse PCA [26].

2.4. Data analysis

Principal component analysis (PCA), as the most popular technique in multivariate analysis, was applied on both hyperspectral image preprocessing and qualitative analysis of fungal growth characteristics in this study. The score plots of vital PCs provided an indication of clustering of groups comprised of similar pixels, and the loading plots of PCA further explained the causes of the internal changes of the five fungi. Support vector machine (SVM) is a learning system that uses a linear function to assume high-dimensional feature space, based on Vapnik's statistical theory for classification and regression problems [27]. And a radial basis function was selected as the kernel function of the SVM using grid optimization method.

In the current study, PCA method and SVM classifier were firstly applied on the average spectra of full wavelength range to study the characteristics of fungal growth process of the five fungi. Then SVM models were established for each fungus respectively to classify its growth days. Moreover, to simplify the SVM classification models, successive projections algorithm (SPA) method was applied to effectively select the optimal wavelengths. With the spectral data of which, multispectral SVM model was established. Finally, the feasibility of early identification of different fungi was checked and corresponding SPA-SVM model was explored based on HSI images of fungi after one day growth.

2.5. Model evaluation

The quality of the developed models was evaluated using confusion matrix, overall accuracy and Kappa coefficient. Confusion matrix can be expressed by Formula 2.

$$M = \begin{bmatrix} m_{11} & m_{12} & \mathrm{L} & m_{1n} \\ m_{21} & m_{22} & \mathrm{L} & m_{2n} \\ \mathrm{L} & \mathrm{L} & \mathrm{L} & \mathrm{L} \\ m_{n1} & m_{n2} & \mathrm{L} & m_{nm} \end{bmatrix} \tag{2}$$

where m_{ij} represents the total number of misjudged samples, and n is the total category of samples. In the matrix, the numbers on the diagonal are the correctly classified numbers, and the higher the number, the better the classification accuracy.

The overall accuracy is the percentage of the correctly classified samples in the total samples in the above confusion matrix, that is, the ratio of the sum of numbers on the diagonal to the sum of all the numbers in the confusion matrix. The calculation formula is as follows:

$$OA = \frac{\sum_{i=1}^{n} m_{ii}}{\sum_{j=1}^{n}\sum_{i=1}^{n} m_{ij}} \tag{3}$$

It can be seen from Formula 3 that the overall accuracy was calculated only by the numbers on the diagonal and the total number of samples, and no other numbers were involved in the matrix. Therefore, the Kappa coefficient was used to confuse the overall information of the matrix.

$$K = \frac{N\sum_{i=1}^{n} m_{ii} - \sum_{i=1}^{n}(m_{i+}m_{+i})}{N^2 - \sum_{i=1}^{n}(m_{i+}m_{+i})} \tag{4}$$

In the Formula 4, n is the actual classification number of samples, and m_{ij} is the value of row i and column j in the confusion matrix, m_{i+} and m_{+i} are the sum of the rows or columns in the confusion matrix respectively, N is the total number of samples. It can be seen from the formula that Kappa coefficient uses the number of each position in the matrix in the calculation process, which can better express the classification effect. Generally, Kappa coefficient is between 0 and 1, and when the value is between 0.80 and 1, it means that the model established has a higher accuracy.

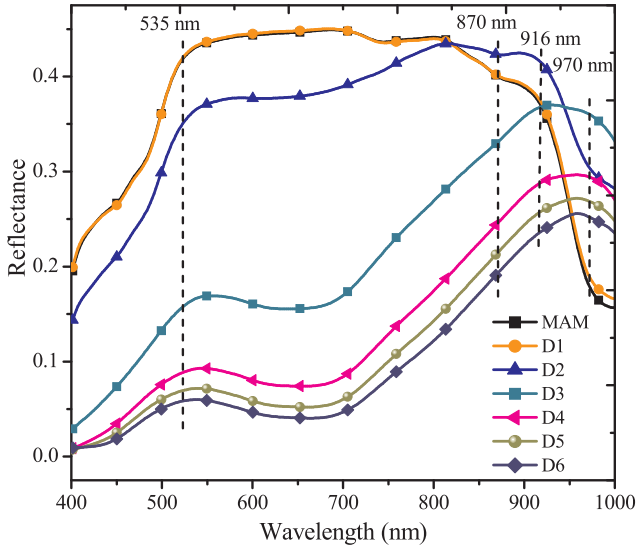

Fig. 2. Average spectra of five fungi on different growth days. (a) Average spectra of *A. parasiticus*; (b) Average spectra of *A. flavus*; (c) Average spectra of *A. niger*; (d) Average spectra of *A. glaucus*; (e) Average spectra of *Penicillium* sp.

3. Results and discussion

3.1. Hyperspectral image data

For convenient observation and comparison of the growth images of different fungi on different days, the hyperspectral image of each fungus on MAM was spliced into a mosaic image according to the time series, Fig. 1 was the resultant growth sequence images with pseudo color image (Red: 641.9 nm, Green: 547.4 nm, Blue: 436.4 nm). As the increase of culture days, the growth trends of the five fungi were generally the same (Fig. 1).

3.2. Fungal growth stages classification

3.2.1. Analysis of fungal growth stage based on spectral characteristics

The original average reflectance spectrum of five fungi cultivated for 6 d were shown in Fig. 2. The spectrum of the first day showed a great similarity with that of the medium when all five fungi have few hyphae visible. Since the surface of the MAM medium exhibited a white color, the control group had the highest reflectance. As the culture days

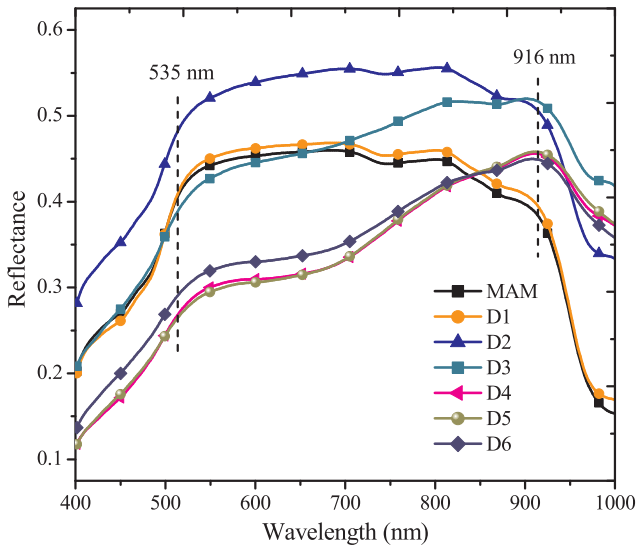

Fig. 2. (*continued*)

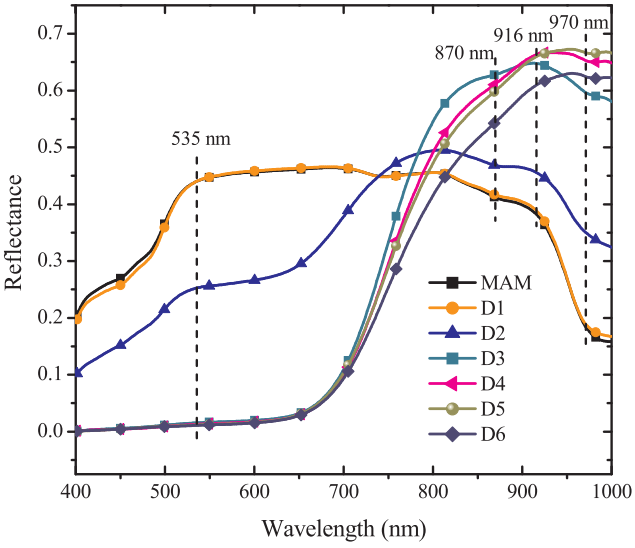

Fig. 2. (*continued*)

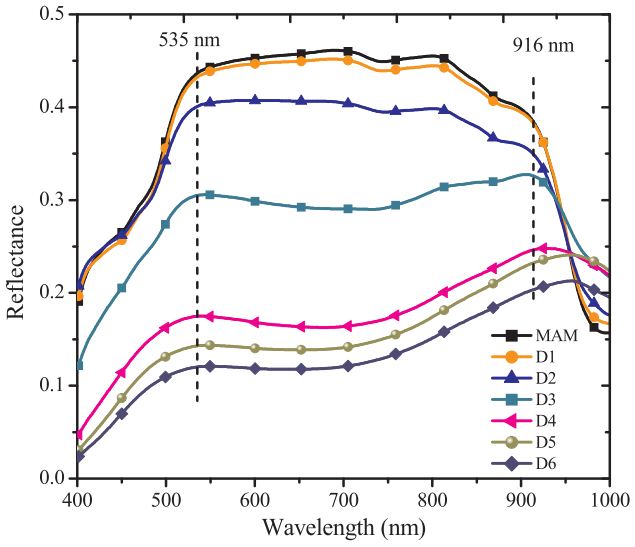

Fig. 2. (*continued*)

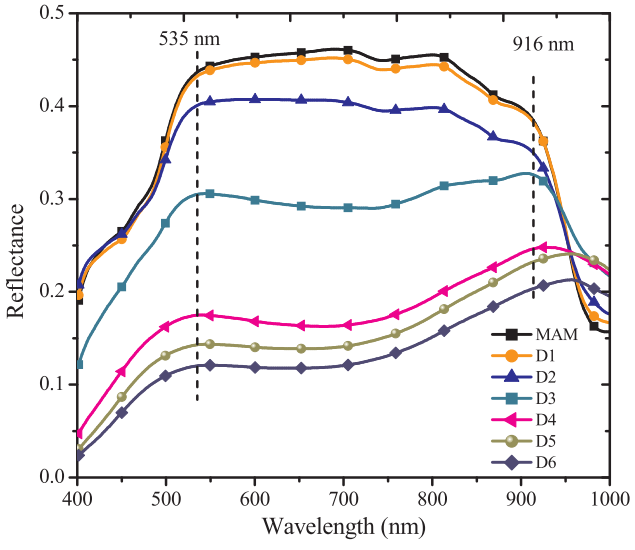

Fig. 2. (*continued*)

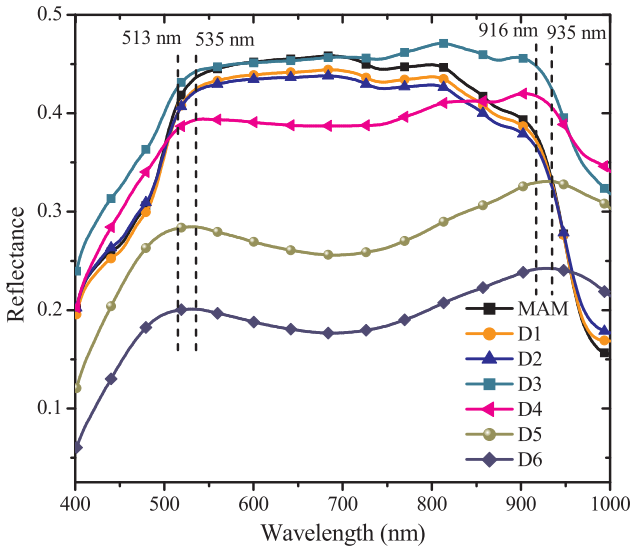

Fig. 2. (*continued*)

progressed, the cascaded hyphae gradually covered the surface of the culture medium, and the reflectance of the spectrum decreased day by day. Thereafter, the colonies begin to show spore color, resulting a sustained reflectance decline. For the four fungi, *A. parasiticus*, *A. flavus*, *A. glaucus* and *Penicillium* sp., no spores were produced in the first three days, only the hyphal density increased, so the reflectance on the third day was smaller than the second day. From days 4 to 6, yellow-green or black-green spores were produced, and the spectral absorption rate increased, thus the reflectance was lower. For *A. niger*, a large number of spores were rapidly produced as soon as colonies appeared from day 3 to 6, whose spectral curve was significantly different from other four fungi seeing from Fig. 2(c).

Also, in the visible range, the medium and spectral curves have obvious peaks at 535 nm, which is related to the pigment of the medium. In the 700–1000 nm band, the peaks at 870, 916, and 970 nm are obvious. 870 nm is related to the third-order overtone of the N-H structure in the protein or in the aromatic ring which is the basic components of the cell wall. The wavelength of 916 nm corresponds to the CH_2 structure and the spectral value at 970 nm was mainly related to the O-H bond expansion and contraction in water molecules [28]. The substances corresponding to these peaks were closely related substances in the process of fungal growth.

3.2.2. Identification of fungal growth days by explanatory PCA

The principal component analysis (PCA) was carried out and the N-dimensional visualization method was used to draw the dispersion map of the selected PCs, forming a multi-dimensional scatter plot (Fig. 3). Take the fastest growing *A. niger* and the most toxic *A. flavus* as examples, a scatter plot was drawn using PC1-PC4, and four different pixel clusters were observed when rotate the 4-dimensional PC subspace, as shown in Fig. 3(a) and (d). Each cluster in the scatter plots corresponds to a pixel with similar PC scores in the captured fungus image. Fig. 3(b) and (e) showed pixels automatically aggregated into different clusters which were marked into different colors. These clusters were then projected onto the original image to form a classified image, the classification map of *A. niger* and *A. flavus* growth stages were shown in Fig. 3(c) and (f) individually. In Fig. 3, the green cluster corresponds to the control group and the fungi on day 1, which mainly representing the culture medium information. The cluster in cyan color is associated with the hyphal growth state on day 2, and the yellow cluster corresponds to freshly germinated spores, while the red cluster corresponds to the mature fungal spores mainly on the day 4 to day 6.

As described in Fig. 3, the sample of control group and day 1 was mainly green, which meant no significant hyphae appeared on the surface of medium. On day 2, the hyphae grew outward from the inside of the medium, and cyan color was coming out, even though there were still green color appeared owing to that the medium was not covered entirely by hyphae. On day 3, the hyphae gradually matured and being more staggered and denser, so that the pixels marked yellow. From day 4 to 6, the spores matured, and the reproduction speed doubled, as a result the whole plate eroded by red.

For the two *Aspergillus* species, *A. niger* grew faster than *A. flavus*, for example, the spores of *A. niger* had already been matured from days 4 to 6, while the picture of *A. flavus* became red little by little. However, the general growth trend of the two fungi was consistent. Thus, the growth process of the two fungi can be divided into four stages on Maize Agar medium. The images of the control group and fungi on the first day were designated as group one; the fungi that grew for two days was labeled as group 2, and the third day to group 3, while the last 4 to 6 days were designated as group 4. In summary, the growth of *A. niger* and *A. flavus* can be roughly divided into four growth stages: control group-D1, D2, D3, D4-D6.

In the same way, to verify the feasibility of the PCA method, the four-dimensional scatter plots of the principal component scores of the other three fungi were also drawn to preliminarily divide its growth days. Similar classification results were shown in Fig. 4. Although the growth details of the five fungi were different, such as growth rate and spore color, their growth patterns over time were generally similar, and can be divided into the same four groups: control group-D1, D2, D3, D4-D6. When inoculated by the pour method, there was a phenomenon of uneven growth of fungi despite the very careful operation, so that an area without fungal growth on the medium existed during the experiment. For example, in the growth stage classification diagram of *Penicillium*, the image on the fourth day had three colors (i.e., green, cyan and yellow colors) that represent the initial growth stages of fungus due to the uneven inoculation. After then, with the rapid growth of the fungus, the area with poor fungal growth was gradually covered. In summary, PCA can be used to distinguish the growth stages of fungi roughly after different days of cultivation.

3.2.3. Establishment of classification model of growing days

3.2.3.1. Regions of interest and data correction. For each type of fungi, region of interests (ROIs) were manually selected on the pretreated hyperspectral images (Fig. 1). In order to extract comprehensive fungi growth information, a 5000-pixel minimum ROI size was targeted for each circular ROI and nine circular ROIs that evenly distributed on the culture dish were created from which the average reflective spectra of ROI of each sample were obtained for data analysis. Since each fungus corresponding to 21 samples, there were 189 (21 samples × 9 ROIs) spectra for each fungus.

3.2.3.2. Full-spectrum classification models of fungal growth days. Classification models for growth days of five fungus species with full-spectrum data were implemented using SVM, which can be utilized to process complex spectral data of these fungus growth data as a nonlinear learning algorithm [29]. For each fungus species, the samples were randomly divided into calibration sets and validation sets with a ratio of 2:1. Therefore, there were a total of 126 samples for all five fungal species in the calibration sets and 63 samples in the validation sets. In the SVM modeling, PC1-PC4 was adopted as the input of the SVM classifier according to the PC segmentation image, and the model was verified by the five-fold cross-validation method. The classification results were shown in Table 2.

Table 2 showed that SVM methods can differentiate different growth days of each fungus species. Due to the difference in growth rate and growth morphology, the accuracy of each fungus was different from each other. Among them, *A. niger* and *A. glaucus* were more rapid in growth rate, and the difference among six days was obvious, so the overall discrimination accuracy was over than 95%. For *A. flavus* and *Penicillium*, the accuracy was both above 90%. Since the difference of *A.*

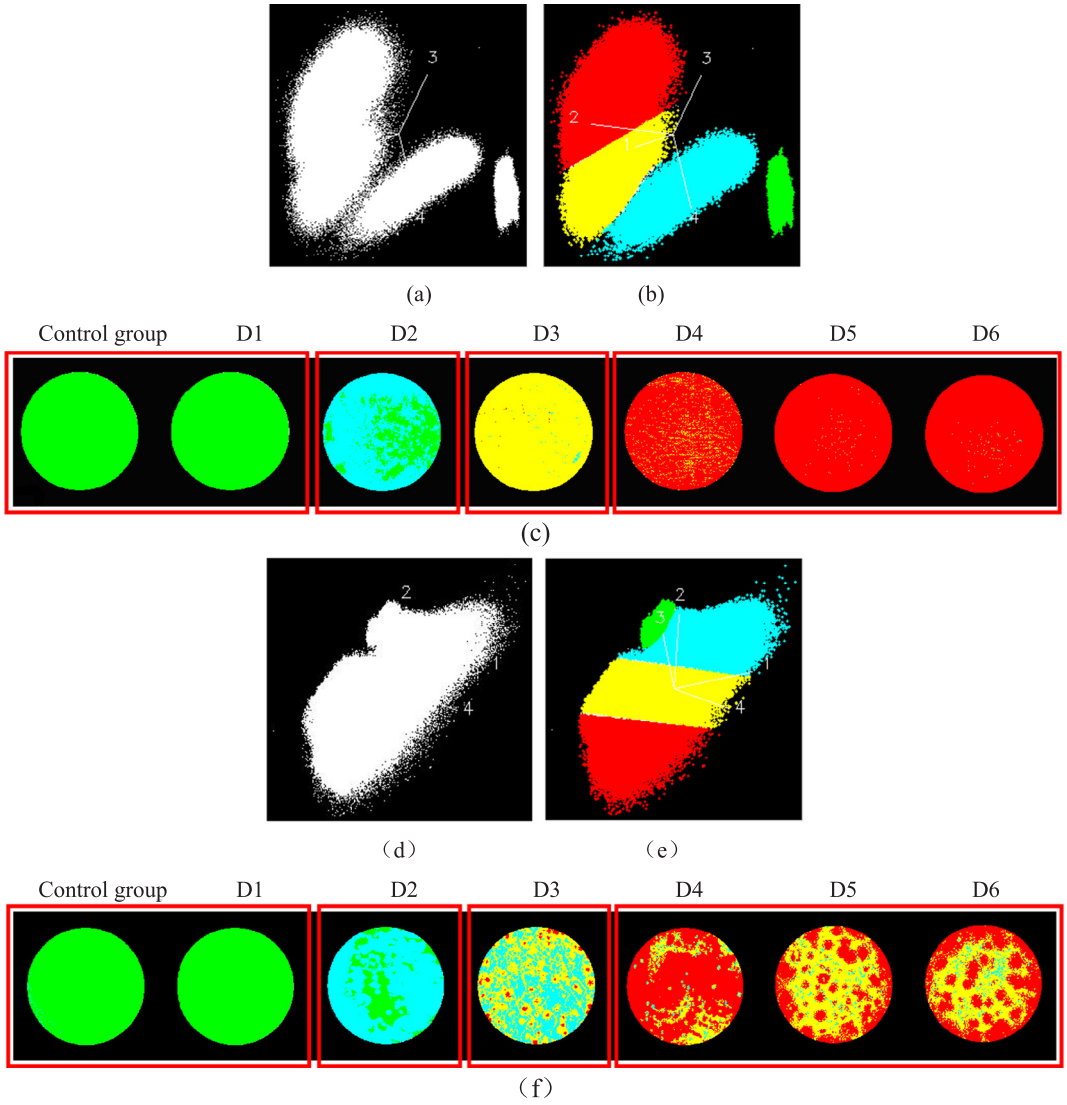

Fig. 3. Scatter plots of *A. niger* (a-c) and *A. flavus* (d-f) and the corresponding images after mapping.

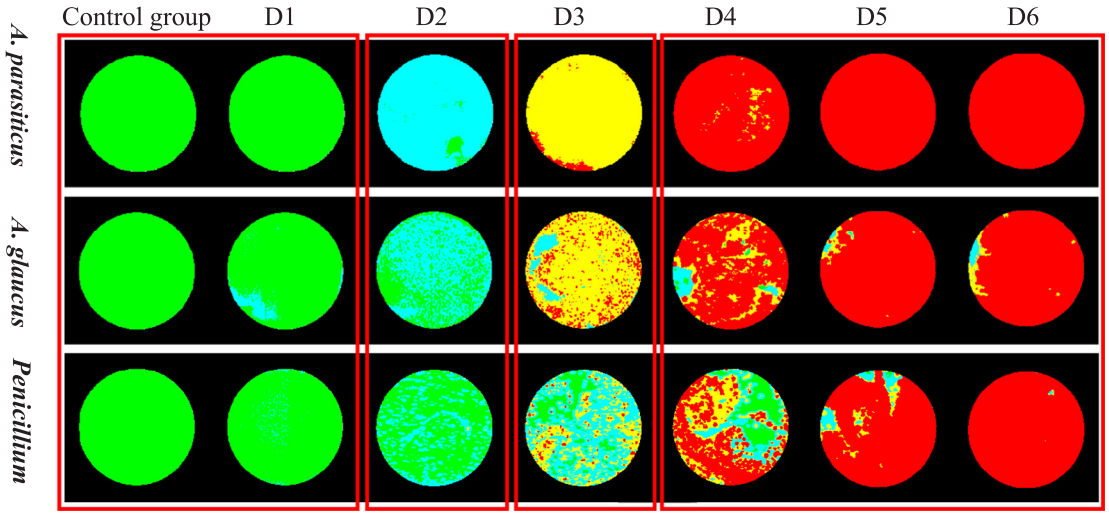

Fig. 4. Classification results of growth stages for the rest three fungi on maize agar medium.

Table 2
Classification results of growth days for the five fungi.

Modeling method	Fungi species	Accuracy/(%)		
		Calibration Set	Validation Set	Cross Validation
PCA-SVM	*A. parasiticus*	88.89	85.52	86.83
	A. flavus	95.85	90.01	92.85
	A. glaucus	97.62	95.71	95.43
	A. niger	99.21	98.41	98.35
	Penicillium	99.45	90.63	91.07

Table 3
Confusion matrix of discriminant result for *A. parasiticus*.

Group	Growth Days						
	Control	D1	D2	D3	D4	D5	D6
Control	27	0	0	0	0	0	0
D1	0	27	0	0	0	0	0
D2	0	0	27	0	0	0	0
D3	0	0	0	27	0	0	0
D4	0	0	0	0	25	1	1
D5	0	0	0	0	1	24	2
D6	0	0	0	0	1	2	24
Accuracy/%	85.71						
Kappa coefficient	0.8916						

parasiticus in last three days were not obvious, it led to a high mis-classification rate, which reduced the overall discriminative accuracy, with accuracy around 85%. It can be concluded that PCA-SVM can identify the growth days of the five fungus species with good accuracy, ranging from 86.83% for *A. parasiticus* and *A. niger* for 98.35% (Table 2).

Further analysis of the mis-classification of growth day data was conducted, taking the *A. parasiticus* as an example, which has the least classification accuracy (86.83%) (Table 3). A confusing matrix of discriminant results was observed. While the model can accurately identify the control group and the fungus on day 1, the mis-classification mainly exists in day 4 to day 6 due to the rapid growth of hyphae and the rapid production of spores.

In particular, identifying the fungi at its early stage of germination was to prevent and control spread of fungi in time, as the fungi had become flourished in from day 4 to day 6, it was meaningless to identify the specific growth days, so mis-classification during this period was allowed.

3.2.3.3. Multispectral classification models. To further simplify the model, the SPA method was used to select the characteristic wavelengths, and a discriminant model based on the spectra at characteristic wavelengths was developed. The optimal characteristic wavelengths of the five fungus species selected by SPA were listed in Table 4.

It is worth to note that a few key wavelengths, e.g., 535, 870, 916, and 970 nm, were selected multiple times among the five fungus species, which were related to the basic fungal cell components, such as,

Table 4
Characteristic wavelengths for five fungi.

Fungi species	Optimal Wavelengths/nm
A. parasiticus	411 534 667 783 869 910 952 970 1000
A. flavus	405 458 480 537 556 615 752 858 872 916
A. glaucus	402 427 530 755 822 871 973 999
A. niger	431 478 503 535 774 913
Penicillium	402 448 521 827 867 967 1000

Table 5
Classification results of fungal growth days based on characteristic wavelengths.

Modeling method	Fungi species	Accuracy/(%)		
		Calibration Set	Validation Set	Cross validation
SPA-SVM	*A. parasiticus*	92.44	90.30	91.26
	A. flavus	97.62	93.65	87.30
	A. glaucus	100	95.87	97.62
	A. niger	99.21	96.83	99.20
	Penicillium	95.87	90.30	91.27

cell wall, oil and moisture in the cells, which is consistent to the analysis in the previous section (Section 3.2.1). Hence, these wavelengths can be used to determine the growth of fungi.

Then based on the spectral data of those selected wavelengths, multispectral classification models were developed for each of the five fungus species (Table 5). The new simplified model improved accuracy, and the variables number is reduced from 284 to 10, which had greatly reduced computation capacity needed for model development.

3.3. Fungal species discrimination after only one day growth

3.3.1. Map feature analysis of the five fungus species

According to the growth characteristics analysis of the five fungus species examined here, it was known that the fungi on the medium started to grow hyphae visually on the second day, and spore characteristics were clear on the fourth day. When multiple fungal infections and mycotoxin contaminations were happened on day four, it was already too late to take effective measures for targeted prevention. Therefore, timely identification of fungal species was of great significance. Thus the fungi grown for one day when the hyphae haven't been visible on the surface were selected to be studied.

Fig. 5 shows the pseudo-color images (Red: 641.9 nm, Green: 547.4 nm, Blue: 436.4 nm) of five fungi that have grown for only one day (24 h). The growth state of the five fungus species was similar, and there were no obvious hyphae shown on the surface. As the result, it was impossible to distinguish fungal types from these images visually.

In order to further classify fungus species in day 1, average spectra of the fungal samples were calculated as shown in Fig. 6. Since the surface of the medium did not show hyphae at all or just appeared very fine hyphae, the average spectrum of the five fungi had great similarity in both spectral and reflectance. Therefore, it was necessary to classify and identify the five fungus species by data statistical analysis methods such as PCA.

The PCA was performed again for this aim based on the average spectral data of all samples (Fig. 7). The contribution rates of the first three PCs were 90.62%, 6.57%, and 1.93%, respectively. Thus the score maps of the first three PCs were shown in Fig. 8, from which the five fungus species can be basically differentiated. Among them, the distinction among *A. glaucus, A. niger* and *Penicillium* sp. was obvious, but *A. parasitiusc* and *A. niger* was partially overlapped that the clustering effect was not obvious. Due to the similarity of growth patterns among these fungus species, the pixel clustering of *A. parasiticus* and *A. niger* easily overlaped, which leads to the poor discrimination between the

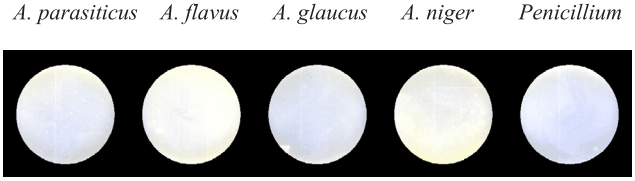

Fig. 5. Pseudo-color images of five fungi in day one.

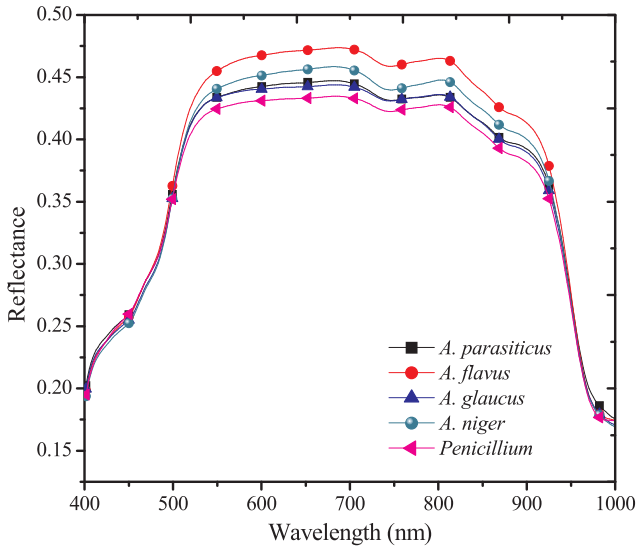

Fig. 6. Average spectra of the five fungi in day one.

two fungi. Therefore, it is impossible to distinguish these fungi only from the cluster of PC scores.

The growth of the five fungi inside the culture medium caused changes in the recorded spectral data, while the first few PCs mostly explained changes in the texture, color, and some internal characteristics of the medium [30]. Therefore, the load factor maps of the first three PCs were plotted to further explain the causes of the internal spectral changes of the five fungal cultures (Fig. 8). Six main wavelengths, 470, 535, 676, 781, 870 and 979 nm, were selected to separate the five fungal species, which was consistent with the wavelengths selected to distinguish fungal growth stages (Section 3.2.1). Wavelengths in the visible region, such as 470, 535 and 676 nm, were related to spectral information associated with color difference. Within the three bands, 470 nm was in the blue region, 535 nm in the green region, and 676 nm in the red region, corresponding to the color of spores. In addition, in the near infrared region, wavelengths of 781, 870 and 979 nm were related to chemical variation among the inoculated five fungi on the same medium. The 781 nm was at the junction of the visible and near-infrared wavelengths, which was important in the process of distinguishing the fungi in culture. Besides the mentioned 870 nm in chapter 3.2.1, the 979 nm was in region of 950–1100 nm, which was related to the second overtone O-H bond [28]. All wavelengths selected above were of vital importance in the separation of the five fungi.

3.3.2. Identification of fungal species based on SVM

The same 9 circular ROIs mentioned were used as the sample data to extract their average spectra. For the collected spectral data, there were 27 samples (9 ROIs × 3 replicates) for each fungus due to three sets of repeated validations, and each group was randomly divided to a ratio of 2:1, with 18 randomly selected as the calibration set and the rest as the verification set. Finally, the calibration set contained a total of 90 (18 per fungi × 5 species) samples, and the validation set contained 45 (9 per fungi × 5 species) samples.

According to the PCA analysis in 3.3.1, PC1-PC3 was selected as the input to the SVM classifier. The stability of the model was verified by five-fold cross-validation method. Results showed that classification accuracy was 100% for calibration, while the validation accuracy was 97.78% and the cross-validation accuracy reached 96.67%, which means the PCA-SVM model can separate fungal species accurately.

In order to simplify the model, the characteristic wavelengths of fungal species identification were further determined by the SPA (Fig. 9). According to the model verification, the calibration rate of model species can reach to 100% only using 7 characteristic wavelengths from total 284 wavelengths. The corresponding wavelengths were 525, 586, 781, 870, 920, 962 and 979 nm chosen by the SPA method, with value of the RMSE being 0.2861 (Fig. 9). Consistent with the wavelengths selected for the model of fungal growth days, the species identification model was also with optimal wavelengths around 535, 870, 916 and 970 nm. On the first day, the growth of the fungi was not obvious, and the color of the medium surface had not shown much difference, which was expressed as the color of the MAM. Therefore, the selected characteristic wavelengths covered most of the bands in the infrared band. Using the model established by the characteristic wavelengths, the accuracy of validation set and cross-validation were 95.56% and 93.33%, respectively. Compared with the classification effect of full-band modeling, the accuracy rate of multispectral model decreased, but there were only eight wavelengths being used, which greatly reduced the amount of computation time.

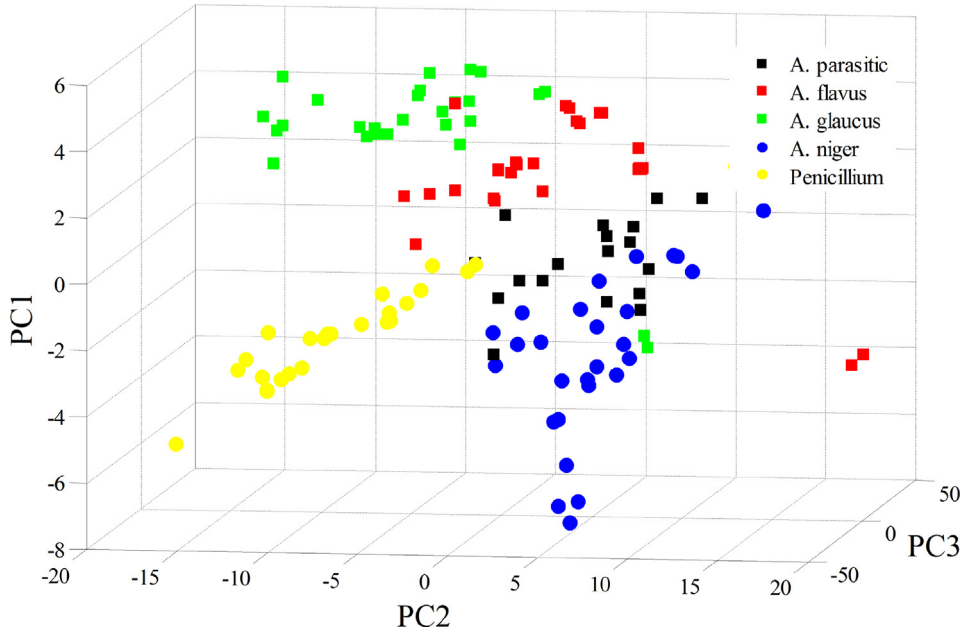

Fig. 7. Scores of the first three PCs.

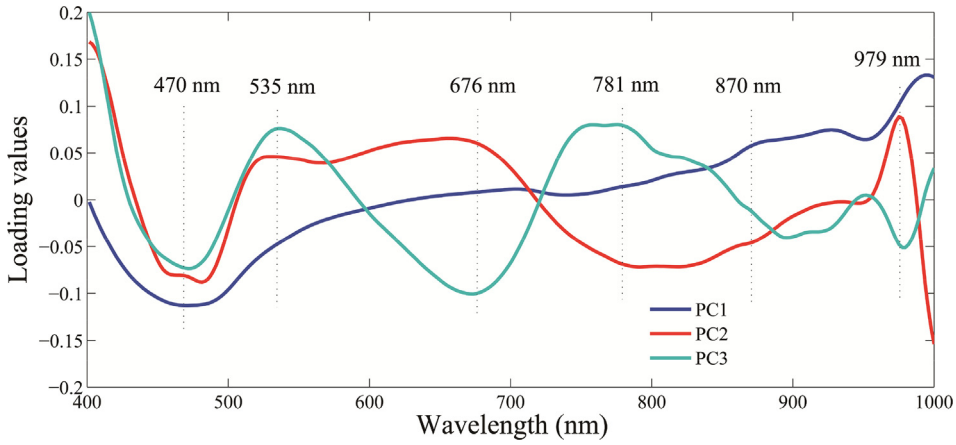

Fig. 8. Loading plots of first three PCs.

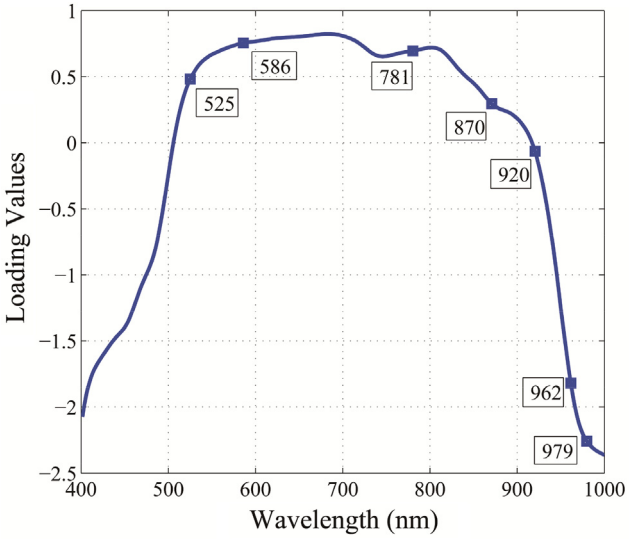

Fig. 9. Characteristic wavelengths selected by SPA.

Table 6
Confusion matrix of classification results for five fungal species.

Group	Fungal Species				
	A. Parasiticus	*A. flavus*	*A. glaucus*	*A. niger*	*Penicillium*
A. Parasiticus	26	0	0	1	0
A. flavus	0	27	0	0	0
A. glaucus	0	0	27	0	0
A. niger	0	0	0	27	0
Penicillium	0	0	0	0	27
Accuracy/%	98.89				
Kappa coefficient	0.9716				

All samples were discriminated using the newly developed model, and the confusion matrix of classification results were shown in Table 6. There were one sample that was mis-identified, that is, the *A. parasiticus* was mis-classified as *A. niger*, which was consistent with the analysis results of the principal component scores. Still, the classification accuracy of 100% and 97.78% could be achieved for the calibration set and the validation set, respectively, and all five fungi were highly separable with average classification accuracy of 98.89% and kappa coefficient of 0.9716, which also verified the robustness of the model and the method proposed in this paper.

4. Conclusions

The dynamic changes in growing characteristics of the five fungi inoculated on Maize Agar medium using Visible/Near-Infrared (Vis/NIR) hyperspectral imaging technique were examined. The findings of the current study are in twofold: classification of fungal growth stages and early identification of fungal species.

(1) Spectral characteristic analysis and principal component analysis were carried out to identify the growth stages of the five fungi qualitatively. According to the four-dimensional score plots and the loading plots, the fungal growth was divided into four growth stages: control group, D1, D2, D3 and D4-D6.
(2) In order to simplify the classification models, PCA-SVM and SPA-SVM models based on five fungal hyperspectral data were established. With overall accuracy higher than 95.71% and kappa coefficient over to 0.8916, the two enhanced models performed the best in describing *A. niger* and *A. glaucus* growth. In addition, key wavelengths of 535, 870, 916 and 970 nm were selected repeatedly, which were critical to differentiate the five fungal species and the initial separation of the five fungi.
(3) HSI images of five fungi after only 24 h growth were extracted and analyzed. The results indicated that the five fungi could be distinguished in one day growth with an average accuracy of 98.89% and kappa coefficient greater than 0.9716. The current study indicated that the visible/near-infrared (Vis/NIR) hyperspectral imaging was a useful tool to assess the growth characteristics of the five fungi that commonly infect the cereal grains.

Declaration of Competing Interest

The authors declare that they have no known competing financial interests or personal relationships that could have appeared to influence the work reported in this paper.

Acknowledgments

This study was funded by the National Key Research and Development Program of China (2018YFC1603500) and the National Natural Science Foundation of China (No. 31772062).

References

[1] J. Gustavsson, C. Cederberg, U. Sonesson, Global Food Losses and Food Waste, FAO, Rome, 2011.
[2] A. Los, D. Ziuzina, P. Bourke, Current and future technologies for microbiological decontamination of cereal grains, J. Food Sci. 83 (2018) 1484–1493, https://doi.org/10.1111/1750-3841.14181.

[3] T. Senthilkumar, D.S. Jayas, N.D.G. White, P.G. Fields, T. Gräfenhan, Detection of ochratoxin a contamination in stored wheat using near-infrared hyperspectral imaging, Infrared Phys. Technol. 81 (2017) 228–235, https://doi.org/10.1016/j.infrared.2017.01.015.
[4] A.D. Fiore, M. Reverberi, A. Ricelli, F. Pinzari, S. Serranti, A.A. Fabbri, G. Bonifazi, C. Fanelli, Early detection of toxigenic fungi on maize by hyperspectral imaging analysis, Int. J. Food Microbiol. 144 (2010) 64–71, https://doi.org/10.1016/j.ijfoodmicro.2010.08.001.
[5] W. Wang, G.W. Heitschmidt, X.Z. Ni, W.R. Windham, S. Hawkins, X. Chu, Identification of aflatoxin b1 on maize kernel surfaces using hyperspectral imaging, Food Control. 42 (2014) 78–86, https://doi.org/10.1016/j.foodcont.2014.01.038.
[6] D. Kimuli, W. Wang, W. Wang, H. Jiang, X. Zhao, X. Chu, Application of swir hyperspectral imaging and chemometrics for identification of aflatoxin b 1, contaminated maize kernels, Infrared Phys. Technol. 89 (2018) 351–362, https://doi.org/10.1016/j.infrared.2018.01.026.
[7] M.K. Saleemi, M.Z. Khan, A. Khan, I. Javed, Z.U.L. Hasan, M.R. Hameed, Occurrence of toxigenic fungi in maize and maize-gluten meal from Pakistan, Phytopathol Mediterr. 51 (2012) 219–224, https://doi.org/10.1080/00103624.2012.675394.
[8] M. Mukanga, J. Derera, P. Tongoona, M.D. Laing, A survey of pre-harvest ear rot diseases of maize and associated mycotoxins in south and central Zambia, Int. J. Food Microbiol. 141 (2010) 213–221, https://doi.org/10.1016/j.ijfoodmicro.2010.05.011.
[9] H. Yao, Z. Hruska, R. Kincaid, R.L. Brown, T.E. Cleveland, Differentiation of toxigenic fungi using hyperspectral imagery, Sens. Instrum. Food Qual. Saf. 2 (2008) 215–224, https://doi.org/10.1007/s11694-008-9055-z.
[10] D. Mcmullin, B. Mizaikoff, R. Krska, Advancements in IR spectroscopic approaches for the determination of fungal derived contaminations in food crops, Anal. Bioanal. Chem. 407 (2015) 653–660, https://doi.org/10.1007/s00216-014-8145-5.
[11] F. Xing, H. Yao, Y. Liu, X. Dai, R.L. Brown, D. Bhatnagar, Recent developments and applications of hyperspectral imaging for rapid detection of mycotoxins and mycotoxigenic fungi in food products, Crit. Rev. Food Sci. Nutr. 59 (2019) 173–180, https://doi.org/10.1080/10408398.2017.1363709.
[12] P. Vermeulen, J.A. Fernández Pierna, H.P. Van Egmond, J. Zegers, P. Dardenne, V. Baeten, Validation and transferability study of a method based on near-infrared hyperspectral imaging for the detection and quantification of ergot bodies in cereals, Anal. Bioanal. Chem. 405 (2013) 7765–7772, https://doi.org/10.1007/s00216-013-6775-7.
[13] A. Plaza, J.A. Benediktsson, J.W. Boardman, J. Brazile, L. Bruzzone, G. Camps-Valls, Recent advances in techniques for hyperspectral image processing, Remote Sens. Environ. 113 (2009) 110–122, https://doi.org/10.1016/j.rse.2007.07.028.
[14] Y. Shao, L. Jiang, H. Zhou, J. Pan, Y. He, Identification of pesticide varieties by testing microalgae using visible/near infrared hyperspectral imaging technology, Sci. Rep. 6 (2016) 24221, https://doi.org/10.1038/srep24221.
[15] W. Wang, X. Ni, K.C. Lawrence, S.C. Yoon, G.W. Heitschmidt, P. Feldner, Feasibility of detecting aflatoxin b1 in single maize kernels using hyperspectral imaging, J. Food Eng. 166 (2015) 182–192, https://doi.org/10.1016/j.jfoodeng.2015.06.009.
[16] P.J. Williams, P. Geladi, T.J. Britz, M. Manley, Investigation of fungal development in maize kernels using nir hyperspectral imaging and multivariate data analysis, J. Cereal Sci. 55 (2012) 272–278, https://doi.org/10.1016/j.jcs.2011.12.003.
[17] X. Chu, W. Wang, S.C. Yoon, X.Z. Ni, G.W. Heitschmidt, Detection of aflatoxin b1 (afb 1) in individual maize kernels using short wave infrared (swir) hyperspectral imaging, Biosyst. Eng. 157 (2017) 13–23, https://doi.org/10.1016/j.biosystemseng.2017.02.005.
[18] P.J. Williams, P. Geladi, J.T. Britz, M. Manley, Near-infrared (NIR) hyperspectral imaging and multivariate image analysis to study growth characteristics and differences between species and strains of members of the genus Fusarium, Anal. Bioanal. Chem. 404 (2012) 1759–1769, https://doi.org/10.1007/s00216-012-6313-z.
[19] P.J. Williams, P. Geladi, T.J. Britz, M. Manley, Growth characteristics of three fusarium species evaluated by near-infrared hyperspectral imaging and multivariate image analysis, Appl. Microbiol. Biotechnol. 96 (2012) 803–813, https://doi.org/10.1007/s00253-012-4380-x.
[20] Y. Sun, X. Gu, Z. Wang, Y. Huang, Y. Wei, M. Zhang, Growth Simulation and Discrimination of Botrytis cinerea, Rhizopus stolonifer and Colletotrichum acutatum using hyperspectral reflectance imaging, PLoS ONE. 10 (2015) e0143400, https://doi.org/10.1371/journal.pone.0143400.
[21] J. Jin, L. Tang, Z. Hruska, H. Yao, Classification of toxigenic and atoxigenic strains of Aspergillus flavus with hyperspectral imaging, Comput. Electron. Agric. 69 (2009) 158–164, https://doi.org/10.1016/j.compag.2009.07.023.
[22] K. Dégardin, A. Guillemain, N.V. Guerreiro, Y. Roggo, Near infrared spectroscopy for counterfeit detection using a large database of pharmaceutical tablets, J. Pharm. Biomed. Anal. 128 (2016) 89–97, https://doi.org/10.1016/j.jpba.2016.05.004.
[23] D. Kimuli, W. Wang, H. Jiang, X. Zhao, X. Chu, Y. Yang, B. Jia, Evaluation of growth characteristics of a mixed culture of toxigenic fungi by Visible/Near-infrared hyperspectral imaging, ASABE (2018).
[24] X. Chu, W. Wang, X. Ni, H. Zheng, X. Zhao, R. Zhang, Y. Li, Growth Identification of *Aspergillus flavus* and *Aspergillus parasiticus* by Visible/Near-Infrared Hyperspectral Imaging, App. Sci. 8 (2018) 513–525, https://doi.org/10.3390/app8040513.
[25] X. Chu, Hyperspectral Imaging Identifications for Cereal Fungi and Detection Methods for Moldy Maize Kernels, China Agricultural University, Beijing, 2018.
[26] G. Chen, S.E. Qian, S. Gleason, Denoising of hyperspectral imagery by combining pca with block-matching 3-d filtering, Can. J. Remote Sens. 37 (2012) 590–595, https://doi.org/10.5589/m12-002.
[27] P.S. Gromski, E. Correa, A.A. Vaughan, et al., A comparison of different chemometrics approaches for the robust classification of electronic nose data, Anal. Bioanal. Chem. 406 (2014) 7581–7590, https://doi.org/10.1007/s00216-014-8216-7.
[28] B.H. Stuart, Infrared spectroscopy: fundamentals and applications, Exp. Thermodyn. 41 (2004) 325–385, https://doi.org/10.1002/0470011149.ch7.
[29] Y. Guo, X.X. Ding, Y.N. Ni, The combination of nir spectroscopy and hplc chromatography for differentiating lotus seed cultivars and quantitative prediction of four main constituents in lotus with the aid of chemometrics, Anal. Methods 9 (2017) 6420–6429, https://doi.org/10.1039/C7AY02021J.
[30] M.A. Shahin, S.J. Symons, Detection of fusarium damaged kernels in canada western red spring wheat using visible/near-infrared hyperspectral imaging and principal component analysis, Comput. Electron Agric. 75 (2011) 107–112, https://doi.org/10.1016/j.compag.2010.10.004.